Surface-driven actuation: Sign reversal under load and surface load-memory effect

Ling-Zhi Liu,[1,2,*] Nadiia Mameka,[1] Jürgen Markmann,[1,3] Hai-Jun Jin,[2] and Jörg Weissmüller[3,1]

[1]*Institute of Materials Research, Materials Mechanics, Helmholtz-Zentrum Geesthacht, 21502 Geesthacht, Germany*

[2]*Shenyang National Laboratory for Materials Science, Institute of Metal Research, Chinese Academy of Sciences, 110016 Shenyang, People's Republic of China*

[3]*Institute of Materials Physics and Technology, Hamburg University of Technology, 21073 Hamburg, Germany*

(Received 7 March 2019; published 24 June 2019)

Motivated by suggestions that hybrid nanomaterials from nanoporous metal and aqueous electrolyte can be used as actuators, we study the impact of an external load on the actuation behavior of nanoporous gold impregnated with aqueous electrolyte. At no load, we observe the well-documented trend for a more positive electrode potential prompting elongation of the nanoporous body. For purely capacitive electrode processes we confirm that the elastic response to external load is simply superimposed on the potential-induced elongation, so that the strain per electric charge is invariant with the load. The observations so far are consistent with the expectation for surface-stress driven actuation in a linear elastic materials system. Surprisingly, however, actuation in the regime of oxygen electrosorption responds strongly to loading: as the load is increased, the strain per charge gradually drops to zero and even inverts its direction. In other words, the actuator moves backward when asked to do work against a substantial external load. Furthermore, we demonstrate that the length change in response to lifting the oxygen adsorbate layer depends on the load that was present at the instant of oxysorption. This "load memory effect" has analogies to shape-memory behavior in massive alloys. Yet, contrary to shape-memory alloys, the microscopic origin is here a surface phase transition. We argue that the observation is a signature of the reorientation of local surface domains with anisotropic surface stress, and that the required atomic transport process acts only while mobile adatoms are supplied during the deposition or lifting of the oxygen adsorbate layer.

DOI: 10.1103/PhysRevMaterials.3.066001

Nanoporous metals are distinguished by their large specific surface area, which can form the basis of materials design strategies providing novel functional behavior [1–4]. As one example, electrochemically driven actuation with nanoporous metals has been thoroughly studied [1,5–8]. Here the pore space is impregnated with electrolyte, and an electric potential bias between the ionic conduction channel in the electrolyte and the electronic channel in the metal excites space-charge or adsorbate layers at the pore surfaces that change a capillary force, the surface stress. The compensating stresses in the bulk of the porous solid result in a macroscopic strain that can reach magnitudes up to about 1% [5], a significant value for a stiff actuator. The phenomenon is well understood in terms of known concepts of the mechanics of porous solids [1,9] and of the coupling between surface stress and superficial charge density [10]. So far, the relevant work focuses on actuation in the absence of external load. Here we explore more practical scenarios where the porous solid does work against load. Using nanoporous gold as the actuator material, we find that the impact of the load depends on the electrode process. During capacitive processes the actuation amplitude is invariant with the load, consistent with the expectation for linear elasticity. Yet for electrosorption of oxygen species our observations have no straightforward explanation in terms of the established concepts of nanoporous metal actuation. Instead, the findings suggest that electric potential cycles induce cyclic atomic reordering at the surface that couples strongly and in an unexpected way to the loading state.

Actuation with nanoporous metal rests on the variation of the surface stress f at the pore surfaces with the superficial charge density q through $\delta f = \varsigma \delta q$. The electrocapillary coupling coefficient ς is characteristic of the underlying electrode process, capacitive charging or pseudocapacitive electrosorption of various anions [11,12]. Mechanical equilibrium requires compensating stresses in the bulk. Hooke's law in turn requires strain, and the effective macroscopic average $\delta\varepsilon$ of the strain variation, projected on the load axis, makes up the actuation. If there is no external load, then $\delta\varepsilon = c\alpha(\nu - 1)Y^{-1}\delta f$ [9] with α, ν, and Y the area of surface per solid volume, Poisson's number, and Young's modulus of the solid phase, respectively. The dimensionless constant c depends on the geometry of the porous microstructure [9,13,14].

The elastic reaction of a macroscopic body of porous solid to uniaxial external load (per cross-sectional area) σ is quantified by the effective Young's modulus Y_{eff} so that $\varepsilon = \sigma / Y_{\text{eff}}$. In porous materials, Y_{eff} can be drastically lower than for massive solids. For nanoporous gold (NPG), Y_{eff} can be varied substantially by plastically deforming the porous material to various degrees [17–20]. Besides modulating f, cycling the electrode potential in an actuation experiment at constant load also prompts significant cyclic changes in Y_{eff} [21]. At constant load, and to first order in the variations of f

*lingzhi.liu@hzg.de; lzliu@imr.ac.cn

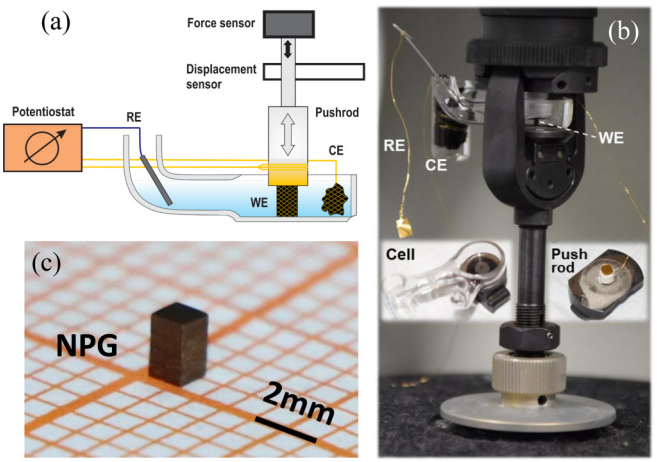

FIG. 1. Experimental setup for the *in situ* dynamic mechanical analysis (DMA). (a) Schematic [15] and (b) a photo [16] of the *in situ* DMA setup equipped with an electrochemical cell. WE: working electrode; RE: reference electrode; CE: counter electrode. (c) A photo of a bulk nanoporous gold sample used in this study. Dimensions: $1.2 \times 1.2 \times 2$ mm^3.

and Y_{eff}, the strain along the load axis then varies as

$$\delta\varepsilon = -c\alpha\frac{1-\nu}{Y}\delta f - \frac{\sigma}{Y_{\text{eff}}^2}\delta Y_{\text{eff}}. \tag{1}$$

Thus, the net actuation strain combines a first contribution that depends on the variation of the surface stress and is independent of the applied stress, plus a second contribution that arises from the variation of stiffness and that scales linearly with the applied stress. Note the sign conventions, negative-valued σ and ε in response to compressive load.

The samples of our study, NPG prepared by electrochemical dealloying [22], feature a bicontinuous microstructure with interconnected networks of pores and solid "ligaments" and can be made in millimeter dimensions [23,24]. This study was performed on cuboid samples with dimensions of $1.2 \times 1.2 \times 2$ mm^3, as displayed in Fig. 1(c). The scanning electron micrograph in Fig. 2(a) shows the microstructure of as-prepared NPG. The image was taken from the cleavage surface of a bulk NPG specimen; it is representative of the structure in the sample interior. The feature size in the image suggests a mean ligament diameter of 40 nm, which means the diameter of ligament cross sections. And this was determined by averaging on more than 100 ligaments measured manually in SEM images.

Figure 2(b) shows a cyclic voltammogram of NPG, indicating capacitive polarization of the clean gold surface at more negative values of the electrode potential E and oxygen species electrosorption peaks at more positive E. Electrosorption of OH^- is known to involve up to one molecular monolayer [25]. Our experiments focused on potential values of 0.3

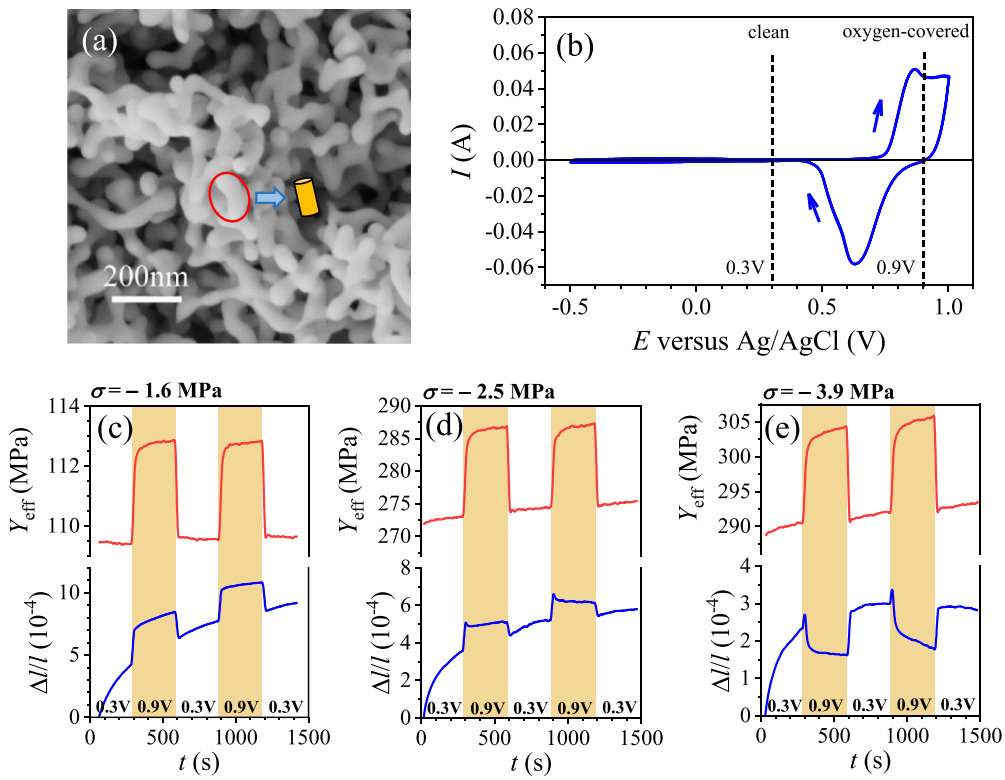

FIG. 2. Microstructure, cyclic voltammetry, and actuation behavior under load for nanoporous gold. (a) Scanning electron micrograph showing cleavage surface of as-prepared sample with average ligament diameter 40 nm. The ligament in NPG is represented by a cylinder, as depicted by the superimposed geometrics in yellow. (b) Cyclic voltammogram of current I versus electrode potential E at scan rate of 5 mV/s. Arrows: Scan direction. Five successive cycles are shown; traces superimpose. (c)–(e) Effective Young's modulus Y_{eff} and macroscopic relative length change $\Delta l/l$ versus time t during cyclic potential jumps at various constant applied compressive stress values σ as indicated in each subfigure.

and 0.9 V versus pseudo Ag/AgCl, representative of the clean and the oxygen-covered surface, respectively.

Electrochemical actuation was characterized by a dynamic mechanical analyzer (DMA) equipped with a custom-built *in situ* electrochemical cell, as presented in Fig. 1 [16]. An NPG sample was placed in a glass cell on a gold plate, and loaded on top by a quartz pushrod for a DMA test. The NPG sample is the working electrode; we used a pseudo Ag/AgCl reference electrode and a wrapped carbon cloth as counter electrode. Gold wires were used for all connections in electrolyte. The master alloy sample was carefully pressed and cut to ensure flat and parallel surfaces on top and bottom; they were then dealloyed. Preloading before compression also improves the contact between the pushrod and the sample.

Compressive loads were superimposed during elastic strain cycles, and macroscopic relative length change ε and the real part Y_{eff} of the effective Young's modulus recorded versus time. The strain frequency in our experiments was 1 Hz, unless otherwise stated. Measurements of Y_{eff} for NPG by DMA have been reported previously and validated by comparison to conventional compression tests [19–22,26].

Prior to exploring actuation in the DMA, the samples were predeformed by loading *in situ* at $\sigma = -6$ MPa [22], which is within the extended elastic-plastic transition regime of NPG [17,18]. This served to minimize creep during the actuation under load. Samples were then subjected to lesser loads and immediately underwent repeated jumps of E between 0.3 and 0.9 V. Figures 2(c)–2(e) show representative traces of Y_{eff} and ε during that procedure. The graphs are distinguished by the applied compressive load σ, which is constant in each figure but increases in magnitude from 1.6 to 3.9 MPa between Figs. 2(c)–2(e).

The graphs of Y_{eff} in Figs. 2(c)–2(e) show that the cyclic potential variation prompts a cyclic variation of the sample stiffness, with 3%–5% stiffening during adsorption of oxygen species. This is consistent with previous observations of electrochemically induced modulation of the stiffness of NPG, a consequence of the variation of the surface excess elastic parameters at the pore walls during oxygen electrosorption [21]. Besides the 1 Hz strain cycles of Fig. 2 we have also explored the frequency regime from 20 Hz down to 20 mHz and consistently found stiffening upon oxygen adsorption [22]. The variation of the apparent *absolute* values of Y_{eff} in Figs. 2(c)–2(e) with σ may arise from mechanical contact problems at low load. Yet, the measurements of *relative* change in stiffness and of length change should not be affected, and indeed the relative variation of Y_{eff} emerges sensibly independent of the load.

Figures 2(c)–2(e) also show that, contrary to the stiffness, the actuation strain depends strongly on σ. At $\sigma = -1.6$ MPa, oxygen electrosorption brings expansion and the strain amplitude is $\delta\varepsilon \sim 0.02\%$. This is similar to reported actuation amplitudes of NPG measured by dilatometry at very small load and under otherwise comparable conditions [13]. When the load is increased to $\sigma = -2.5$ MPa, $\delta\varepsilon$ is significantly diminished. Furthermore, the strain transients for the adsorption events now develop a small overshoot. When the load is raised further to $\sigma = -3.9$ MPa, the overshoot becomes more pronounced and, most remarkably, the net strain has changed sign and now exhibits contraction during adsorption. In other words, the data show that the actuator will move backward when asked to do work against a substantial applied load.

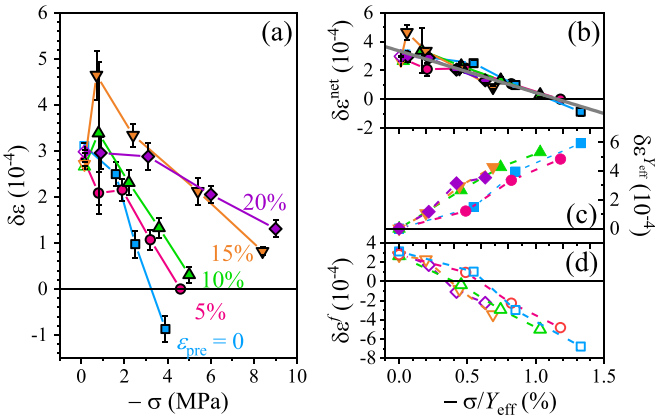

FIG. 3. Dependence of the actuation strain on the loading condition. (a) Actuation strain $\delta\varepsilon$ during potential jumps (0.3 ↔ 0.9 V) versus applied stress σ for samples predeformed by different (essentially plastic) strains as indicated by labels. Error bars: Standard deviation from a series of successive jumps. Half-empty symbols: Values measured in dilatometer at low load. (b)–(d) Actuation strain plotted versus $-\sigma/Y_{\text{eff}}$, the stress normalized to Young's modulus. (b) Net actuation strain, as in (a). Note that all data are now following the identical trendline. (c) Contribution of δY_{eff}, i.e., second term in Eq. (1), to $\delta\varepsilon$. (d) Subtracting the data in (c) from that in (b) yields the contribution from δf, i.e., first term in Eq. (1) to $\delta\varepsilon$.

Superimposed on the reversible strain of actuation, Figs. 2(c)–2(e) show a slow irreversible expansion. This is readily explained as a viscoelastic response when NPG is relieved from the larger compressive stress of the predeformation that preceded this experiment. A small irreversible variation of Y_{eff} appears as well. We speculate that this effect may arise from local deformation at the loaded surfaces, which improves the contact. The magnitude of this change in stiffness is negligible compared with the cyclic variation of Y_{eff} upon potential jumps and so does not affect our observations.

Figure 3(a) plots the actuation strain in response to the $0.3 \rightarrow 0.9$ V potential jump versus σ. The plot compiles data from samples which were plastically predeformed [22] so as to produce different solid fractions and, consequently, different Y_{eff}. The samples were also examined *in situ* in a dilatometer under the smaller load of -0.14 MPa, and this data are included in the figure. The graphs for different predeformation differ substantially, yet Fig. 3(b) shows that all results coincide on a single straight line when plotted versus σ/Y_{eff}. Since σ/Y_{eff} is simply the static strain induced by the applied load, the result suggests that the load dependence of the actuation behavior is inherently linked to the elastic strain.

We have used the experimental data for δY_{eff} from experiments such as Figs. 2(c)–2(e) along with the second term on the right-hand side of Eq. (1) for estimating the contribution of δY_{eff} to the net actuation strain $\delta\varepsilon$. The result, Fig. 3(c), confirms that the stiffening during oxygen species electrosorption contributes an expansion to the net actuation strain. Subtracting that contribution from the net $\delta\varepsilon$ yields the contribution from δf to the actuation strain, that is, the first term on the right-hand side of Eq. (1). Figure 3(d)

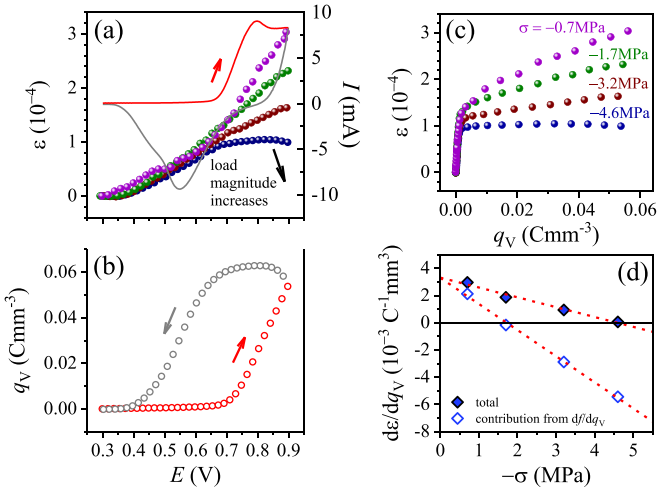

FIG. 4. Actuation during cyclic potential sweeps including capacitive and oxygen electrosorption processes. (a) Right ordinate and lines: Cyclic voltammogram of current I versus potential E at scan rate 10 mV/s (red arrow denotes scan direction; red graph: anodic branch). Left ordinate and symbols: Strain ε versus E in the anodic scan at various loads. No systematic changes are resolved between CV under different loads. (b) Transferred volumetric charge density q_V versus E. Anodic part is shown in red. (c) Plot of ε versus q_V at various loads, using symbols as in (a). (d) Effective strain-charge coefficient $d\varepsilon/dq_V$ during oxygen electrosorption versus the applied stress σ. Closed symbols: Net value. Open symbols: Contribution from surface stress variation, after subtraction of contribution from Young's modulus variation, as in Fig. 3. Dashed lines: Linear regression. Sample was predeformed to compressive strain of 5%.

shows that this contribution changes sign at comparatively low external strain (∼0.5%), and that the strain contribution from δf becomes large and negative with increasing load. The net actuation strain is then a subtle balance between two contributions of opposite sign, expansion due to stiffening and contraction due to surface stress change.

Besides the potential *jumps*, we found it instructive to also study strain during cyclic potential *sweeps* under various loads. In these studies we also included potential variations in the capacitive regime, at more negative values of E. As can be seen in Fig. 4(a), the strain here varies linearly with the potential, with different slopes for capacitive versus oxygen electrosorption processes. Furthermore, the slope during oxygen adsorption confirms the trend discussed above, with progressively lessening expansion and finally contraction during positive-going potential as the compressive load is increased.

Remarkably, Fig. 4(a) shows that the load has no effect on the potential-strain response during capacitive cycles. This observation suggests that in the capacitive regime (i) the stiffness is sensibly independent of the potential and (ii) the surface stress is sensibly independent of the load. The observation on stiffness is indeed consistent with previous results [21]. Clearly the load sensitivity of the actuation is linked specifically to oxygen adsorption.

Since surface stress changes are inherently linked to the superficial charge density (as opposed to its energy-conjugate variable, the electrode potential), we have also integrated the current to obtain the charge transferred to the porous body [Fig. 4(b)], and we display strain versus charge at the various loads in Fig. 4(c). This representation emphasizes the actuation in the regime of oxygen adsorption, where most of the charge is transferred. The graphs are essentially linear in that regime, with a noticeable but small curvature. We have extracted their slope—in other words, the load-dependent strain-charge coefficients in the oxysorption regime—by linear regression. The closed symbols in Fig. 4(d) display the results; they are seen to agree with the trends discussed so far. No significant changes were resolved between cyclic voltammograms recorded in different loading states [22]. In other words, the superficial charge density and the amount of adsorption are sensibly independent of the load.

Our discussion of the data in Fig. 3(b) suggests that the load dependence of the actuation strain is linked to the elastic strain in the porous body. In view of Eq. (1) we are then led to conclude that the sign of the electrocapillary coupling coefficient ς during oxygen adsorption on gold is sensitive to the local strain at the surface. Next, we inspect two possible hypotheses for the origin of this strain dependence.

Our first hypothesis is that strain prompts a transformation between two distinct surface phases, each with isotropic surface stress but with different magnitudes of f and ς. This hypothesis appears dissatisfactory because a discontinuous transformation between distinct phases is poorly compatible with (i) the gradual variation of ς with strain, and (ii) the constant values of stiffness and electrosorption charge (recall that the cyclic voltammetry resolves no change in superficial charge density between the various loading states), independent of the strain.

The second hypothesis, which rests on observations of low symmetry surface reconstructions on many solid surfaces and specifically on gold, adopts the notion of reorientation of surface domains of one and the same phase but with an anisotropic surface stress tensor.

The pairing row reconstruction of the Si(100) surface is an example for a low-symmetry surface reconstruction with anisotropic surface stress. Its surface stress components parallel and perpendicular to the so-called dimer bands are of opposite sign [27,28]. When a uniaxial strain is imposed in the surface plane, the coverage of the surface by domains aligned parallel or perpendicular to the strain axis varies linearly with the strain magnitude [27]. As illustrated in Fig. 5, domains tend to align their axis of more positive surface stress (tensile stress state in the surface) with the direction of more compressive applied strain. Since the macroscopic mean stress and strain in the bulk are governed by averages over the surface stress tensors [29], the reorientation reduces the magnitude of the net bulk stress in the compressive strain direction. This implies an enhanced compliance, along with a strain-dependent mean projected surface stress. Our observations are consistent with a process of this type. We emphasize that the local elastic deformation of the ligaments in NPG under a compressive stress is mostly bending [17]. In other words, when the surface on one side of a ligament is under compression, with a raised surface stress in the reconstruction, its opposite side is stretched, with a reduced surface stress. These effects cooperate to amplify the bending strain.

Bulk-terminated or reconstructed (110) surface of metals provides further examples of anisotropic surface stress [30].

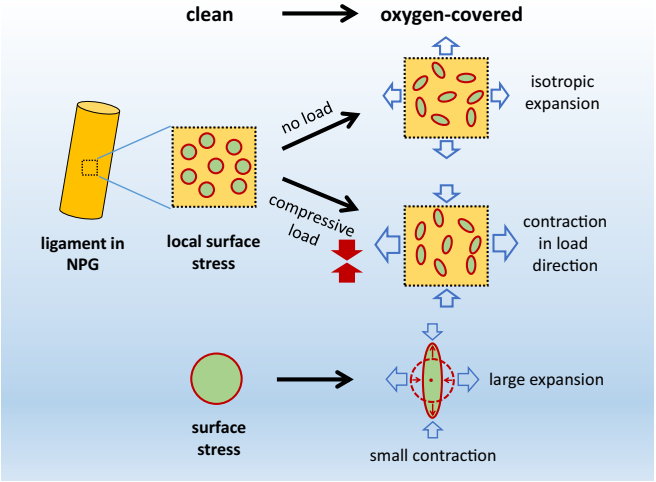

FIG. 5. Schematics for surface reconstruction induced by oxygen adsorption on surfaces of NPG with or without external load. Dashed-outline squares represent a local ligament surface region in NPG. Circles and ellipses in green indicate isotropy or anisotropy, respectively, of surface stress in regions of different stress state. Closed arrows: Direction of the applied external load. Open arrows: Direction of actuation strain; the size denotes the relative magnitude.

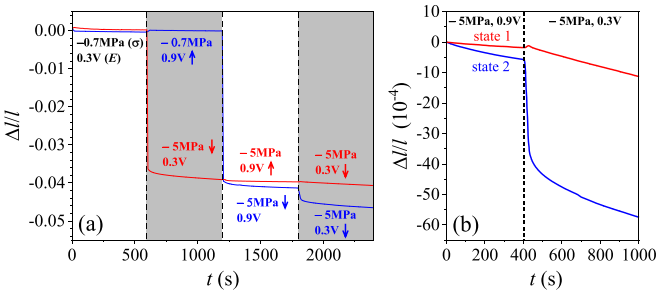

FIG. 6. Demonstration for a "load memory" effect. (a) Relative length change versus time during two independent successive load and potential jumps. Upward and downward arrows denote increase and decrease of the parameters (E and σ), respectively. (b) The strain variation of the two states versus time around the last potential jump in (a), i.e., from 0.9 to 0.3 V at $\sigma = -5$ MPa. The dashed line indicates the potential jump. Colors of the curves agree with those in (a).

Terraces of clean Au(111) can undergo a herringbone reconstruction by compression along the $\langle\bar{1}10\rangle$ direction [31,32], providing yet another low-symmetry surface with anisotropic surface stress. Investigations of the surface stress during electrochemical potential cycles indicate that clean Au surfaces are bulk terminated under the conditions of our experiment [33]. Yet, upon oxygen adsorption Au(111) can reconstruct to a "striped phase" of twofold symmetry [34,35]. These observations at least rule in structures with anisotropic surface stress on oxygen-covered surfaces of our samples.

The roughness and curvature of the pore surfaces of NPG may prevent systematic, long-range ordered reconstruction. Yet, curvature requires step edges, which are again the source of anisotropic surface stress. It is well known that stress dipoles are associated with steps, mediating their mutual elastic interaction [28,36,37]. While these dipoles do not induce net long-range stress or strain, it was recently demonstrated that step edges also exhibit line stresses that do contribute to the mean surface stress [38]. These stresses again have twofold in-plane symmetry. It is therefore conceivable that oxygen adsorption brings a decoration of step edges with oxygen, changing their stress state, along with a reorganization of the surface step population that acts similarly as the domain reorganization in strained reconstructed surfaces. A drastic reorganization is indeed well documented in the context of CO oxidation catalysis at metal surfaces, including those of nanoporous gold, where high-resolution transmission electron microscopy reveals cyclic transitions between faceted (few step edges) and rough (many step edges), depending on which species dominantly covers the surface [39,40].

The reorientation of low symmetry surface configurations brings enhanced elastic compliance. How is this compatible with our observation of stiffening upon oxygen adsorption? We note that the stiffening is observed at all strain frequencies in the DMA, down to 0.02 Hz [22]—it shows no sign of enhanced compliance even when there is ample time for rearrangement. This suggests that the mechanism which brings the enhanced compliance acts only during the short intervals when the oxygen coverage is changed. This notion is indeed supported by the well-known phenomenon that oxygen ad- or desorption on gold sets free small mobile clusters or single adatoms of gold which bring a transient enhancement of the kinetics of structural rearrangement [34,35,41–43]. Time-dependent studies of surface stress variation after oxygen adsorption on gold have confirmed that a transient restructuring after the adsorption is relevant for surface stress [12,44]. Details of the time dependence, $\varsigma < 0$ for fast and $\varsigma > 0$ for slower processes, in those studies are consistent with the initial overshoot of the strain after oxygen adsorption in Figs. 2(d) and 2(e).

We have suggested a picture where a static applied load and the structural rearrangement in response to oxygen electrosorption provide the kinetics for reordering that allows local surface stress states of low symmetry to align with the direction of the load. As a consequence of this picture one would expect that adsorbing oxygen at no load and applying the static external load *after* the adsorption process—that is, when the short period of enhanced mobility is already over—would prevent the reordering. Figure 6 demonstrates that this is indeed born out by experiment.

Figure 6(a) shows strain versus time for two load/potential histories, starting with the clean surface at low load and then either applying first the load and then the oxidizing potential jump (state 1, red graph) or first the potential and then the load (state 2, blue graph). Both samples are then in nominally the same condition, at load and oxidized. Yet, when the potential jumps to the negative direction, reducing the surface oxide [Fig. 6(b)], the two samples react in a drastically different manner: the "state 1" sample undergoes a small expansion, consistent with the lifting of a stress-aligned domain structure, whereas the "state 2" sample contracts by a much larger amount. The behavior of state 2 is compatible with the scenario of standard actuation strain under no load being superimposed by the strain due to stiffness change at load.

Clearly the loaded and oxygen-covered state has a memory of the loading condition at the instant of oxidation. This "load memory" effect has analogies to the shape memory effect of certain alloys and polymers, where temperature changes initiate a (martensitic) phase transformation in the bulk and, along with it, a strain recovery that memorizes shape before the transformation [45].

Our actuation experiments on nanoporous gold confirm that the surface-induced strain in response to double-layer charging on clean surfaces remains invariant when an external load is applied, consistent with expectations based on linear elasticity. Surprisingly, however, the actuation strain in response to oxygen adsorption drops to zero and even inverts its direction as more and more external load is applied. From a technological point of view, this is bad news for actuation with NPG since an actuator that cannot work against load is of little practical use. Yet, from a more fundamental point of view, our observations reveal an intriguing surface phenomenon, where the state of the surface can depend on the load that was present at the instant of oxidation—in other words, a surface-load memory effect. We find the observations consistent with the presence of anisotropic surface stress states and with the notion that surface domains reorient according to the local stress or strain direction that is imposed by the external load. The kinetics of the reorientation is provided by and dependent on the transient extra atomic mobility that accompanies the reaction of the gold surface with oxygen, explaining why the load at the instant of oxidation is decisive.

ACKNOWLEDGMENT

This work was supported by the German Research Foundation (DFG), Grant We1424/16-1.

[1] J. Weissmüller, R. N. Viswanath, D. Kramer, P. Zimmer, R. Würschum, and H. Gleiter, Charge-induced reversible strain in a metal, Science **300**, 312 (2003).

[2] J. Weissmüller and K. Sieradzki, Dealloyed nanoporous materials with interface-controlled behavior, MRS Bull. **43**, 14 (2018).

[3] Q. Chen, Y. Ding, and M. Chen, Nanoporous metal by dealloying for electrochemical energy conversion and storage, MRS Bull. **43**, 43 (2018).

[4] E. Şžeker, W.-C. Shih, and K. J. Stine, Nanoporous metals by alloy corrosion: Bioanalytical and biomedical applications, MRS Bull. **43**, 49 (2018).

[5] H.-J. Jin, X.-L. Wang, S. Parida, K. Wang, M. Seo, and J. Weissmüller, Nanoporous Au-Pt alloys as large strain electrochemical actuators, Nano Lett. **10**, 187 (2009).

[6] E. Detsi, Z. G. Chen, W. P. Vellinga, P. R. Onck, and J. T. M. De Hosson, Actuating and sensing properties of nanoporous gold, J. Nanoscience Nanotechnol. **12**, 4951 (2012).

[7] C. Cheng and A. H. W. Ngan, Reversible electrochemical actuation of metallic nanohoneycombs induced by pseudocapacitive redox processes, ACS Nano **9**, 3984 (2015).

[8] Q. Bai, C. Si, J. Zhang, and Z. Zhang, Sign inversion of surface stress-charge response of bulk nanoporous nickel actuators with different surface states, Phys. Chem. Chem. Phys. **18**, 19798 (2016).

[9] J. Weissmüller, H. L. Duan, and D. Farkas, Deformation of solids with nanoscale pores by the action of capillary forces, Acta Mater. **58**, 1 (2010).

[10] Y. Umeno, C. Elsässer, B. Meyer, P. Gumbsch, M. Nothacker, J. Weißmüller, and F. Evers, Ab initio study of surface stress response to charging, Europhys. Lett. **78**, 13001 (2007).

[11] W. Haiss, Surface stress of clean and adsorbate-covered solids, Rep. Prog. Phys. **64**, 591 (2001).

[12] Q. Deng and J. Weissmüller, Electrocapillary coupling during electrosorption, Langmuir **30**, 10522 (2014).

[13] L. H. Shao, H. J. Jin, R. N. Viswanath, and J. Weissmüller, Different measures for the capillarity-driven deformation of a nanoporous metal, Europhys. Lett. **89**, 66001 (2010).

[14] F. Liu, X.-L. Ye, and H.-J. Jin, Anomalous low strain induced by surface charge in nanoporous gold with low relative density, Phys. Chem. Chem. Phys. **19**, 19217 (2017).

[15] N. Mameka, Surface-controlled mechanical properties of bulk nanoporous gold, Dissertation, Hamburg University of Technology, 2016, https://doi.org/10.15480/882.1328.

[16] S. Shi, J. Markmann, and J. Weissmüller, Verifying Larché–Cahn elasticity, a milestone of 20th-century thermodynamics, Proc. Natl. Acad. Sci. USA **115**, 10914 (2018).

[17] N. Huber, R. N. Viswanath, N. Mameka, J. Markmann, and J. Weißmüller, Scaling laws of nanoporous metals under uniaxial compression, Acta Mater. **67**, 252 (2014).

[18] B.-N. D. Ngô, A. Stukowski, N. Mameka, J. Markmann, K. Albe, and J. Weissmüller, Anomalous compliance and early yielding of nanoporous gold, Acta Mater. **93**, 144 (2015).

[19] L.-Z. Liu, X.-L. Ye, and H.-J. Jin, Interpreting anomalous low-strength and low-stiffness of nanoporous gold: Quantification of network connectivity, Acta Mater. **118**, 77 (2016).

[20] N. Mameka, K. Wang, J. Markmann, E. T. Lilleodden, and J. Weissmüller, Nanoporous gold-testing macro-scale samples to probe small-scale mechanical behavior, Mater. Res. Lett. **4**, 27 (2016).

[21] N. Mameka, J. Markmann, H.-J. Jin, and J. Weissmüller, Electrical stiffness modulation—confirming the impact of surface excess elasticity on the mechanics of nanomaterials, Acta Mater. **76**, 272 (2014).

[22] See Supplemental Material at http://link.aps.org/supplemental/10.1103/PhysRevMaterials.3.066001 for experimental details of sample preparation and testings in this study, and supplementary results of compression and electrochemical *in situ* DMA.

[23] R. Li and K. Sieradzki, Ductile-Brittle Transition in Random Porous Au, Phys. Rev. Lett. **68**, 1168 (1992).

[24] J. Erlebacher, M. J. Aziz, A. Karma, N. Dimitrov, and K. Sieradzki, Evolution of nanoporosity in dealloying, Nature (London) **410**, 450 (2001).

[25] H. Angerstein-Kozlowska, B. E. Conway, A. Hamelin, and L. Stoicoviciu, Elementary steps of electrochemical oxidation of single-crystal planes of Au part II. A chemical and structural

basis of oxidation of the (111) plane, J. Electroanal. Chem. Interfacial Electrochem. **228**, 429 (1987).

[26] L.-Z. Liu and H.-J. Jin, Scaling equation for the elastic modulus of nanoporous gold with "fixed" network connectivity, Appl. Phys. Lett. **110**, 211902 (2017).

[27] F. K. Men, W. E. Packard, and M. B. Webb, Si(100) Surface Under an Externally Applied Stress, Phys. Rev. Lett. **61**, 2469 (1988).

[28] O. L. Alerhand, D. Vanderbilt, R. D. Meade, and J. D. Joannopoulos, Spontaneous Formation of Stress Domains on Crystal Surfaces, Phys. Rev. Lett. **61**, 1973 (1988).

[29] J. Weissmüller and J. W. Cahn, Mean stresses in microstructures due to interface stresses: A generalization of a capillary equation for solids, Acta Mater. **45**, 1899 (1997).

[30] S. Olivier, G. Tréglia, A. Saúl, and F. Willaime, Influence of surface stress in the missing row reconstruction of fcc transition metals, Surf. Sci. **600**, 5131 (2006).

[31] J. V. Barth, H. Brune, G. Ertl, and R. J. Behm, Scanning tunneling microscopy observations on the reconstructed Au (111) surface: Atomic structure, long-range superstructure, rotational domains, and surface defects, Phys. Rev. B **42**, 9307 (1990).

[32] S. Narasimhan and D. Vanderbilt, Elastic Stress Domains and the Herringbone Reconstruction on Au(111), Phys. Rev. Lett. **69**, 1564 (1992).

[33] H. Ibach, C. E. Bach, M. Giesen, and A. Grossmann, Potential-induced stress in the solid-liquid interface: Au (111) and Au (100) in an $HClO_4$ electrolyte, Surf. Sci. **375**, 107 (1997).

[34] B. K. Min, X. Deng, D. Pinnaduwage, R. Schalek, and C. M. Friend, Oxygen-induced restructuring with release of gold atoms from Au (111), Phys. Rev. B **72**, 121410(R) (2005).

[35] B. K. Min, A. R. Alemozafar, M. M. Biener, J. Biener, and C. M. Friend, Reaction of Au(111) with sulfur and oxygen: Scanning tunneling microscopic study, Top. Catal. **36**, 77 (2005).

[36] V. I. Marchenko and A. Y. Parshin, Elastic properties of crystal surfaces, Sov. Phys. JETP **52**, 129 (1980).

[37] P. Müller and A. Saúl, Elastic effects on surface physics, Surf. Sci. Rep. **54**, 157 (2004).

[38] W. N. Li, H. L. Duan, K. Albe, and J. Weissmüller, Line stress of step edges at crystal surfaces, Surf. Sci. **605**, 947 (2011).

[39] S. B. Vendelbo, C. F. Elkjær, H. Falsig, I. Puspitasari, P. Dona, L. Mele, B. Morana, B. J. Nelissen, R. van Rijn, J. F. Creemer, P. J. Kooyman, and S. Helveg, Visualization of oscillatory behaviour of Pt nanoparticles catalysing Co oxidation, Nat. Mater. **13**, 884 (2014).

[40] N. Kamiuchi, K. Sun, R. Aso, M. Tane, T. Tamaoka, H. Yoshida, and S. Takeda, Self-activated surface dynamics in gold catalysts under reaction environments, Nat. Commun. **9**, 2060 (2018).

[41] D. J. Trevor, C. E. D. Chidsey, and D. N. Loiacono, *In Situ* Scanning-Tunneling-Microscope Observation of Roughening, Annealing, and Dissolution of Gold (111) in an Electrochemical Cell, Phys. Rev. Lett. **62**, 929 (1989).

[42] C. M. Vitus and A. J. Davenport, *In-situ* scanning-tunneling-microscopy studies of the formation and reduction of a gold oxide monolayer on Au(111), J. Electrochem. Soc. **141**, 1291 (1994).

[43] M. A. Schneeweiss and D. M. Kolb, Oxide formation on Au(111)—An *in situ* STM study, Solid State Ionics **94**, 171 (1997).

[44] Q. Deng, V. Gopal, and J. Weissmüller, Less noble or more noble: How strain affects the binding of oxygen on gold, Angew. Chem. **127**, 13173 (2015).

[45] K. Otsuka and C. M. Wayman, *Shape Memory Materials* (Cambridge University Press, Cambridge, 1999).